Anomaly in the radial breathing mode of resonant Raman scattering from vertically aligned single-walled carbon nanotube films

Zhengyi Zhang,[1,2] Erik Einarsson,[1] Yoichi Murakami,[3]
Yuhei Miyauchi,[4,5] Shigeo Maruyama[1*]

[1]*Department of Mechanical Engineering,*
The University of Tokyo, 7-3-1 Hongo,
Bunkyo-ku, Tokyo 113-8656, Japan

[2]*Department of Mechanical Engineering,*
Columbia University, New York, NY 10027, USA

[3]*Global Edge Institute, Tokyo Institute of Technology,*
2-12-1 Ookayama, Meguro-ku, Tokyo 152-8550, Japan

[4]*Institute for Chemical Research, Kyoto University, Uji, Kyoto 611-0011, Japan*

[5]*Departments of Physics and Electrical Engineering,*
Columbia University, New York, NY 10027, USA

(Dated: September 24, 2009)

Abstract

Polarization-dependent resonance Raman spectra of a single-walled carbon nanotube (SWNT) array were measured such that the polarization of the scattered light was selected either parallel or perpendicular to that of the incident light. For the parallel configuration, radial breathing mode (RBM) peaks exhibited two different polarization dependencies. One group (dominated by a peak at 203 cm^{-1}) had a maximum scattering intensity for incident light parallel to the alignment direction, whereas the other group (dominated by a peak at 181 cm^{-1}) had maximum intensity for excitation perpendicular to the alignment direction. This anomaly has been attributed to resonance with non-vertical transitions due to perpendicularly polarized excitation [Y. Murakami *et al.*, Phys. Rev. B **71**, 085403 (2005)]. Decomposing the Raman spectra and comparing to theoretical expectations for the two different configurations revealed that the 203 cm^{-1} group peaks behave as expected for parallel-polarized dipole excitation, whereas the 181 cm^{-1} group peaks deviate significantly from the prediction assuming perpendicularly polarized excitation. Furthermore, after correcting the spectra for laser-induced heating effects, the 181 cm^{-1} group peak intensities were found to be essentially independent of polarization angle. The sound interpretation of these results is that the RBM anomaly is due to the parallel excitation of 'stray' SWNTs suspended within the vertically aligned array.

I. INTRODUCTION

There has been great interest in the optical properties of single-walled carbon nanotubes (SWNTs) due to their quasi-one-dimensionality. Divergences in the electronic density of states, so-called van Hove singularities, give rise to the dominant $E_{\mu,\mu}$ inter-subband transitions (where μ denotes the cutting line index[1]) for incident light polarized along the nanotube axis. However, cross-polarized absorption by SWNTs has been measured by photoluminescence excitation (PLE) spectroscopy,[2,3] which is possible by non-vertical ($E_{\mu,\mu\pm1}$) transitions to neighboring cutting lines.[4] Anisotropy in optical absorption spectra has also been studied[5,6] and used to determine the nematic order parameter, indicating the degree of alignment of SWNTs. Separate parallel and perpendicular π plasmons have also been identified in the UV region.[6,7]

It has been previously reported[8] that vertically aligned single-walled carbon nanotubes (VA-SWNTs) synthesized by the alcohol catalytic chemical vapor deposition (ACCVD) method[9] exhibit a characteristic Raman peak in the radial breathing mode (RBM) region at approximately 181 cm^{-1} for excitation with 488 nm light. Contrary to expectation, the intensity of this peak was strongest for incident light polarized *perpendicular* to the VA-SWNT alignment direction. Other weaker peaks were also found to exhibit the same unexpected behavior. Furthermore, these peaks could not be accurately assigned to specific (n, m) chiralities by comparing to calculations of interband transition energies (the so-called Kataura plot). They were thus attributed[8] to a resonance with $E_{\mu,\mu\pm1}$, which is allowed for perpendicularly polarized excitation.[4] It has been known for some time that excitons are responsible for the optical properties of SWNTs.[10,11] However, the band-model concept of cutting lines and selection rules for interband transitions, on which the polarized Raman discussion is based, are still valid. To clarify the origin of this RBM anomaly, we systematically measured resonance Raman spectra for different polarization conditions, and quantitatively analyzed the spectra using theoretical models and an updated Kataura plot. Our findings indicate the differing polarization dependencies arise not from perpendicularly polarized excitation of SWNTs, but from the morphology of the VA-SWNT array.

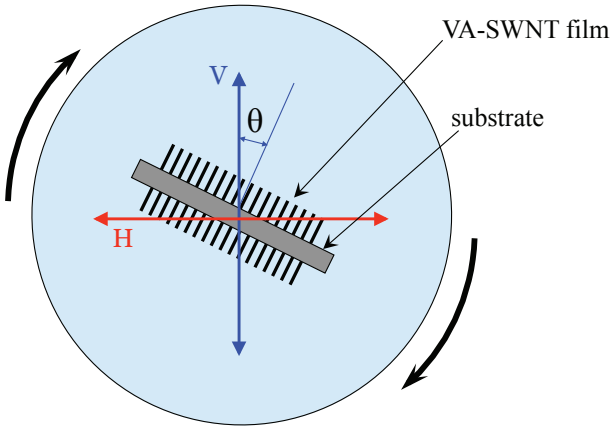

FIG. 1: (Color online) Top view of a rotating stage with mounted VA-SWNT array. Incident light is polarized along V, and a polarizer selects the outgoing polarization along either V or H.

II. EXPERIMENTAL DETAILS

A. Measurement of polarization-dependent Raman spectra

VA-SWNTs were synthesized on a quartz substrate by the ACCVD method, as described in detail elsewhere.[12,13] The substrate was then cleaved to reveal the cross-section of the array, which had a height of approximately 15 μm as determined by SEM observation. For measurement of resonance Raman spectra, this fractured piece was mounted perpendicular to a rotatable stage such that the alignment direction was in the plane of the stage and the linearly polarized excitation laser was incident on the cross-section of the VA-SWNT array.

The two measurement configurations used in these experiments are shown in Fig. 1. The polarization of the incident light was the same for both configurations, but the polarization of the scattered light was selected by changing the orientation of a polarizer placed in the outgoing light path. A scrambler was coupled to the polarizer to prevent polarization-dependent losses in the optical fiber connecting the micro-Raman system and the monochrometer. The VV configuration indicates that the selected polarization of the scattered light has the same orientation as the incident light (i.e., both vertical). Similarly, the VH configuration means the selected polarization of the scattered light is perpendicular to that of the incident light. Once the orientations had been fixed, the angle θ between the incident light polarization and the SWNT alignment direction was changed by rotating the sample stage. Measurements

were made in 15° increments for values of θ from 0 to 90°. Unless otherwise stated, the light source used in all measurements was a 488 nm Ar laser, with a power of 0.2 mW at the sample surface. The diameter of the laser spot was approximately 2 μm.

B. Preparation of stretch-aligned SWNTs

Polarization-dependent resonance Raman spectra of a stretch-aligned SWNT-polymer sample were also obtained for comparison with the VA-SWNT array. The sample was prepared by first mixing 20 mg of purified CoMoCat SWNTs in 10 g of D_2O containing 1 wt% SDBS (*sodium dodecyl benzene sulfonate*). This solution was ultrasonicated with a horn-type ultrasonicator for 30 minutes at a power flux level of 368 W cm^{-2} Following ultrasonication, the dispersion was ultracentrifuged for 1 hour at 163,000 g and the supernatant collected. PVA (poly-vinyl alcohol) powder was dissolved at 15 wt% in 80°C distilled water for 10 minutes, then cooled to room temperature. This was then added into the SWNT suspension and thoroughly mixed. The mixture was poured into a Petri dish and allowed to polymerize at room temperature for 24 hours. The resulting grey solid was then heated to 80°C and gently stretched to four or five times its original length.

III. RESULTS AND DISCUSSIONS

Figure 2 shows a series of resonance Raman spectra obtained for both VV and VH configurations from an as-grown VA-SWNT array. Considering that the position of the laser spot may shift during rotation, values plotted are averages of three independent measurements. In the VV configuration, it can be clearly seen that there are two types of RBM peaks exhibiting opposite polarization dependence: the 160 and 203 cm^{-1} peaks (noted as the {203 cm^{-1}} group) have decreasing intensity with increasing polarization angle θ, whereas the 145, 181, 244, and 256 cm^{-1} peaks (noted as the {181 cm^{-1}} group) increase in intensity as θ approaches 90°.

If all the SWNTs were well aligned, all the RBM peaks should exhibit the same polarization dependence as the {203 cm^{-1}} group, i.e., behave as an antenna. This is observed in polarized absorption and Raman spectra of the stretch-aligned CoMoCat-PVA sample. As shown in Fig. 3(a), the extremely weak optical absorption by perpendicularly polarized light

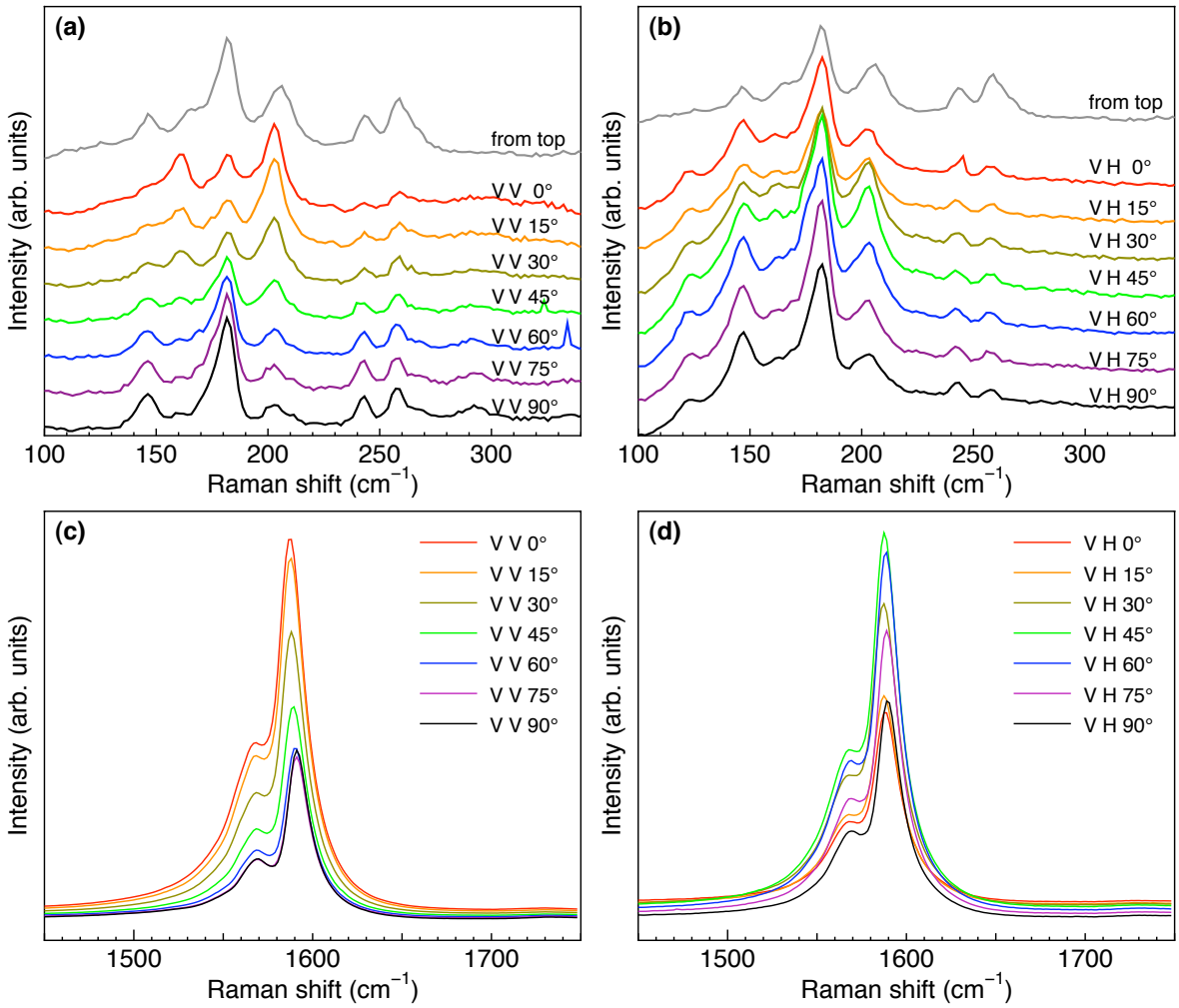

FIG. 2: (Color online) Polarization angle dependence of the RBM (a, b) and G-band (c, d) of a VA-SWNT array for 488 nm laser excitation. The incident polarization angle was changed from 0° (along the alignment direction) to 90° (perpendicular to the alignment direction) in 15° steps. Left and right panels correspond to VV and VH configurations, respectively.

illustrates the so-called 'antenna effect', and yields an order parameter[6,14] $S \approx 0.99$, indicating excellent alignment of CoMoCat SWNTs in the stretched polymer matrix. In polarized Raman spectra with VV or VH configurations, all peaks behave as expected for parallel excitation (see Appendix, Fig. 9). The normalized intensities in both configurations of the G-band peak at 1593 cm^{-1} and the only distinguishable RBM peak at 305 cm^{-1} are plotted in Fig. 3(b) and Fig. 3(c). They agree well with intensity calculations for parallel excitation and an order parameter of approx. 0.9, which is consistent with the result obtained from

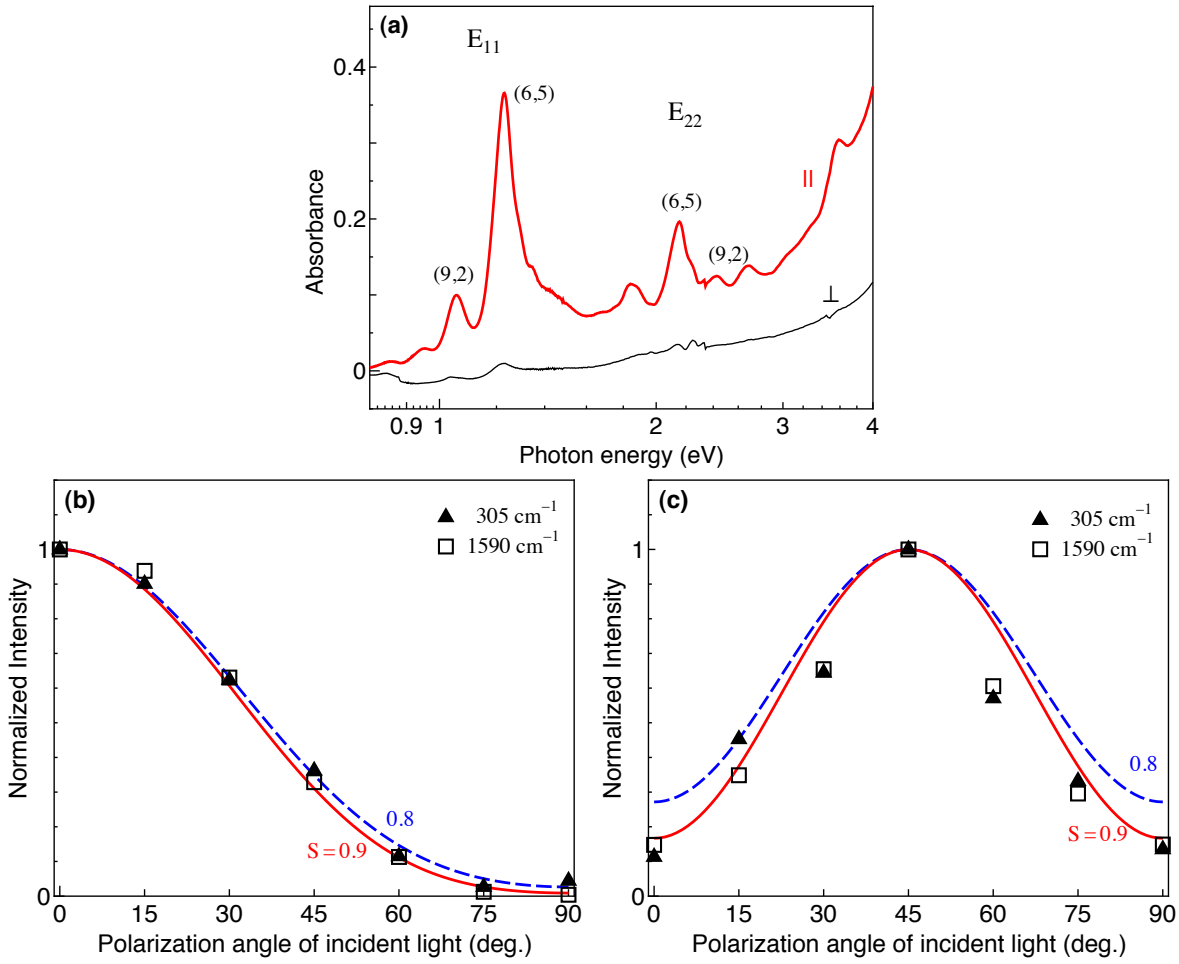

FIG. 3: (Color online) (a) Optical absorption spectra from a stretched CoMoCat-PVA array. Incident light is polarized parallel (∥) and perpendicular (⊥) to the stretching direction. Lower panels show normalized RBM peak intensities as a function of incident light polarization angle for (b) VV and (c) VH configurations. Solid and dashed lines are intensity calculations for parallel excitation assuming different order parameters (see Appendix).

optical absorption.

According to Raman selection rules, the RBM (which has A symmetry) is observable only when the incident and scattered light are either both parallel or both perpendicular to the SWNT axis. Hence, it is possible the {181 cm^{-1}} peaks are due to perpendicularly-polarized excitation of the SWNTs.[4,8] The polarization dependence of each peak's normalized intensity has been plotted to test this hypothesis (see Appendix, Fig. 8). Peak intensities were obtained by decomposing the RBM spectra into a sum of Lorentzian peaks (not shown),

and were then compared to the equation describing the relationship between scattered light intensity and polarization angle for different excitations. Here, we apply the appropriate relations for $I_{VV}^{\parallel\parallel}$ and $I_{VV}^{\perp\perp}$ assuming a Gaussian distribution function and utilizing the nematic order parameter $S = \frac{1}{2}\left(3 < \cos^2\varphi - 1 >\right)$ to indicate the alignment of the SWNTs within the array ($\parallel$ and $\perp$ indicate the incident and scattered polarizations, see Appendix for derivation).

$$I_{VV}^{\parallel\parallel} \propto 2\cos^4\theta\left\langle\cos^4\varphi\right\rangle + 6\cos^2\theta\sin^2\theta\left\langle\sin^2\varphi\cos^2\varphi\right\rangle + \tfrac{3}{4}\sin^4\theta\left\langle\sin^4\varphi\right\rangle \quad (1)$$

$$I_{VV}^{\perp\perp} \propto (8 - 28\sin^2\theta + 23\sin^4\theta)\left\langle\sin^4\varphi\right\rangle + (32\sin^2 - 40\sin^4\theta)\left\langle\sin^2\varphi\right\rangle + 8\sin^4\theta \quad (2)$$

The value $S \approx 0.75$ has been determined for our VA-SWNTs based on both polarization dependent optical absorption[6] and X-ray absorption spectra.[15] One important note is that the G-band peaks were found to slightly increase in frequency when the incident polarization angle changed from 0° to 90°. This is because SWNTs more strongly absorb light that is polarized along the tube axis, causing heating of the entire array and thus affecting both the positions and intensities of the Raman peaks.[16] To correct for the heating effect, we measured the intensities of five RBM peaks under different temperatures (see Appendix, Fig. 10). The corrected intensities of the 181 cm^{-1} group with polarization angle are shown in Fig. 4.

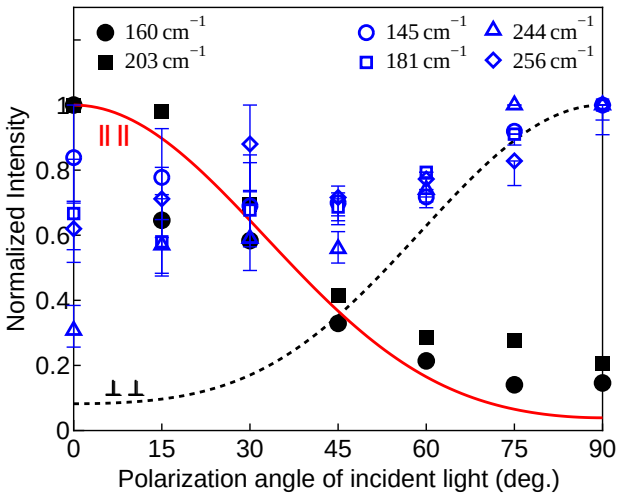

FIG. 4: (Color online) Polarization-dependence of RBM peak intensities (VV configuration) after correcting for temperature effects. Solid (dashed) lines are calculated intensities expected for parallel (perpendicular) excitation.

It can be seen that the {203 cm^{-1}} group behaves similar to the expectation for parallel excitation. However, the {181 cm^{-1}} group behavior deviates significantly from the assumption of perpendicularly polarized excitation, and is essentially independent of polarization angle. For the VH configuration (Appendix, Fig. 8(b)), both parallel and perpendicularly-polarized excitations have intensity maxima at 45°. As with the VV configuration, however, the {181 cm^{-1}} group deviates significantly from the VH expectation for perpendicularly polarized excitation.

These deviations lead us to consider another possible origin of this anomaly. We attemped to assign these peaks using a Kataura plot showing $E_{\mu,\mu}$ transitions (from the ith cutting line in the valence band to the ith cutting line in the conduction band) using the relation $\omega_{\mathrm{RBM}} = \frac{217.8}{d_t} + 15.7$ cm^{-1} (d_t is the SWNT diameter in nm), which had been determined from fitting of experimentally obtained data.[17] The area of interest is shown in Fig. 5.

Here we plot the RBM peaks found in polarized Raman spectra obtained with 488, 514 and 633 nm excitation (spectra for 633 nm excitation were obtained using the same method as described in Section II, and the 514 nm measurement results are from Ref. [8].) Peaks exhibiting the antenna effect are indicated by a diamond, and those exhibiting different behavior are indicated by a cross. Considering the bundle-induced broadening of the resonance window (up to 120 meV),[18] and referring to the resonance Raman scattering map in Ref. [17], nearly every peak can be assigned to E_{ii} transitions.

High-resolution Raman spectra (Fig. 6(a)) reveal that the strong 181 cm^{-1} peak is actually composed of three or four sharp peaks. This corresponds the family of SWNTs near 181 cm^{-1}. Similar narrow, high-intensity peaks have been observed previously for isolated SWNTs.[19] It has also been found that the intensities of these peaks slowly decrease,[8] and essentially disappear after storage in air for a long period of time (i.e., months or years). However, these peaks can be recovered (Fig. 6(b)) by heating the sample at 300°C for 10 minutes. This suggests adsorption of molecules onto the SWNT (here, primarily H_2O), is responsible for the change in peak intensity. Interestingly, the {181 cm^{-1}} group peaks disappear if the alignment of the SWNTs is disturbed, e.g., by dispersing in D_2O and drying. These peaks cannot be recovered by heating, etc., although the {203 cm^{-1}} group remains. This shows that the {181 cm^{-1}} group is morphology dependent, and simultaneously sensitive to the environment. High resolution SEM images give us a closer look at the array (Appendix, Fig. 11(a)), revealing the existence of these small bundles or isolated SWNTs suspended

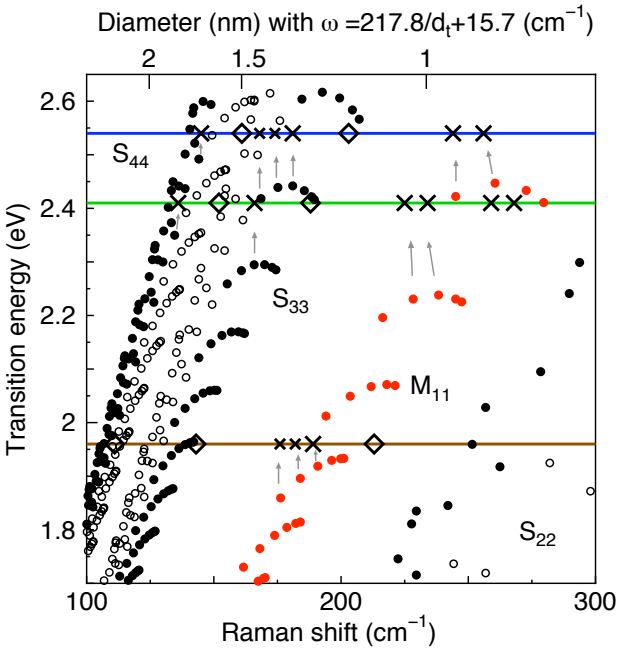

FIG. 5: (Color online) Kataura plot showing E_{ii} transition energies. SWNT diameter and Raman shift are related by the equation $\omega_{\mathrm{RBM}} = \frac{217.8}{d_t} + 15.7$ (cm^{-1}). Red filled circles denote metallic $[(2n+m)\mathrm{mod}3 = 0]$ SWNTs, while black open and black filled circles represent type-I $[(2n+m)\mathrm{mod}3 = 1]$ and type-II $[(2n+m)\mathrm{mod}3 = 2]$ semiconducting SWNTs, respectively. The solid blue, green and brown lines denote the 2.54, 2.41 and 1.96 eV excitation energies of the 488, 514 and 633 nm lasers used to obtain spectra. Diamonds denote peaks behaving as parallel excitation, and crosses denote peaks exhibiting anomalous behavior.

among the forest of well aligned SWNTs. Very small bundles or individual SWNTs would be very sensitive to adsorption, and formation of bundles by disturbing the morphology could shift their resonance window away from the excitation laser energy.

In the Kataura plot shown in Fig. 5, we noticed that {203 cm^{-1}} group peaks (diamonds) correspond to SWNTs with E_{ii} energies close to the laser excitation energy, which are bundled tubes dominant in the array. The {181 cm^{-1}} group peaks, however, correspond to SWNTs where the E_{ii} energies lie slightly below the laser excitation energy. The key to interpreting these results is considering this Kataura plot is based on experimentally obtained data, i.e., primarily SWNT bundles. The transition energy for an isolated SWNT is relatively blue-shifted from the bundle transition energy. Thus, when the excitation laser light is polarized perpendicular to the SWNT alignment direction and we excite primarily

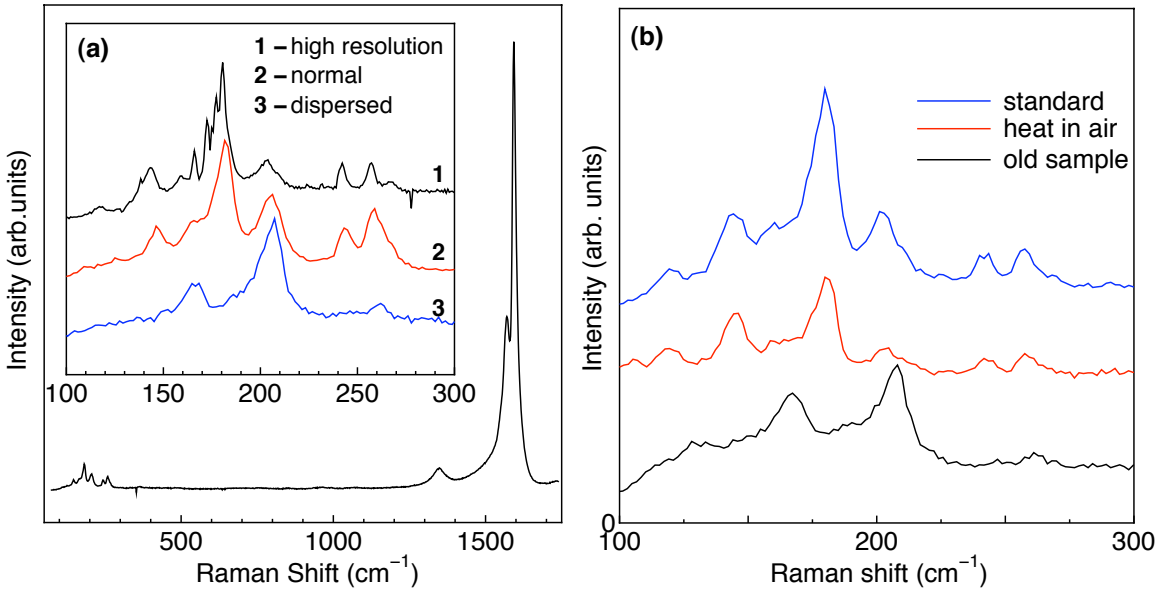

FIG. 6: (Color online) (a) Raman spectra taken from the top of a VA-SWNT array. Inset shows the RBM region with high-resolution (topmost) and with normal resolution before (middle) and after (lower) dispersion in D_2O. (b) RBM spectra taken from top of a VA-SWNT array after synthesis (top), after storage for two years (bottom), and after heating at 300°C (middle).

stray SWNTs, the transition energies will shift upward toward the laser energy, as indicated by the grey arrows, and result in stronger RBM intensities. We thus conclude some 'stray', isolated SWNTs within the array are responsible for the RBM anomaly.

IV. CONCLUSION

Here we address the anomalous behavior of some radial breathing mode peaks found in polarization-dependent resonance Raman spectra of vertically aligned SWNTs. Excitation by perpendicularly polarized light has been previously suggested to explain these findings, but here we show significant deviation from theoretical calculations that make this hypothesis unlikely to be correct. Consideration of temperature-dependent peak intensities shows the anomalous peaks intensities are essentially independent of polarization angle. The presence of isolated SWNTs is evidenced by high-resolution Raman spectra, which show the broad feature at 181 cm^{-1} is actually composed of four sharp peaks. Furthermore, (n, m) assignment using a more recent experimentally obtained Kataura plot shows these peaks

can be identified, and the abnormal behavior is due to the mixture of bundled and individual SWNTs dispersed throughout the vertically aligned array. FE-SEM observation also reveals many small bundles or isolated SWNTs are distributed among the forest. We explain the RBM anomaly as being due to the different resonance windows for dominant vertically aligned bundles and 'stray' SWNTs, which are excited differently based on the relative polarization of the excitation laser.

Acknowledgments

Part of this work was financially supported by Grants-in-Aid for Scientific Research (19206024 and 19054003) from the Japan Society for the Promotion of Science, SCOPE (051403009) from the Ministry of Internal Affairs and Communications, NEDO (Japan), and by the Global COE Program "Global Center for Excellence for Mechanical Systems Innovation", MEXT, Japan. ZZ acknowledges support through the Panasonic Scholarship.

V. APPENDIX

A. Multiple-dipole approximation

1. *Scattering geometry*

The dipole approximation allows for optical transitions between sub-bands of the valence and conduction bands $E^v_\mu \rightarrow E^c_{\mu'}$, where $\mu' = \mu$ for light polarized along the nanotube axis,[1,20] and $\mu' = \mu \pm 1$ for light polarized perpendicular to the nanotube axis.[4] Thus, by changing the light polarization relative to the SWNT it is possible to select different symmetry-allowed phonon modes.[21]

In the following discussion we use the scattering geometry shown in Fig. 7, which is based on that in Ref. [14]. This establishes the z axis as the SWNT alignment direction (i.e., normal to the substrate surface), and assumes that the VA-SWNTs are straight and distributed uniformly about this axis. The orientation of a given SWNT is defined by two angles φ ($0 \leq \varphi \leq \frac{\pi}{2}$), which is the angle between tube axis and z-axis, and γ ($0 \leq \gamma \leq 2\pi$),

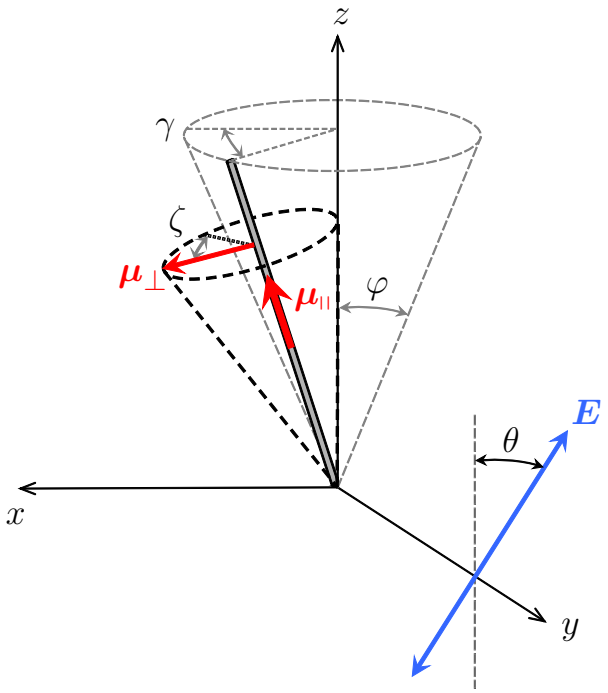

FIG. 7: (Color online) Excitation geometry and orientation of parallel and perpendicular dipoles ($\boldsymbol{\mu}$) for VA-SWNTs with some distribution around the substrate normal (z-axis).

which is the rotational angle of a plane constructed by the SWNT axis and the z-axis. Selection rules allow two dipoles to contribute to the first-order Raman scattering process. These dipoles are oriented parallel ($\boldsymbol{\mu}_{\shortparallel}$) and perpendicular ($\boldsymbol{\mu}_{\perp}$) to the nanotube axis.

2. Approximation of the Raman process

The Raman scattering process can be approximated as absorption and emission of photons, where the emission process is simply time-reversed absorption. Here we use this approximation, taking into account contributions from multiple dipoles.

As described in section II, we adopt two configurations, VV and VH, to measure spectra for different scattering geometries. According to the selection rules, the RBM (A mode) can only be seen when incident and scattered light are parallel or perpendicular to the tube axis. Thus, we discuss these two cases below, using the notation "$\parallel\parallel$" and "$\perp\perp$".

We first consider the case of only one SWNT in the VV configuration. If the scattered light is polarized along the SWNT axis, the observed intensity $I_{VV}^{\parallel\parallel}$ is described by

$$I_{VV}^{\parallel\parallel} \propto I_{\mathrm{in}}|\boldsymbol{E}\cdot\boldsymbol{\mu}_{\shortparallel}|^2\, I_{\mathrm{sc}}|\boldsymbol{\mu}_{\shortparallel}\cdot\boldsymbol{E}|^2, \tag{3}$$

where I_{in} and I_{sc} are the respective intensities of the incident and scattered light, and the electric field vector $\boldsymbol{E}$ of the incident photon, expressed by $\boldsymbol{E} = (-\sin\theta, 0, \cos\theta)$, only has components in the x-z plane. Taking into account the distribution of the SWNTs we obtain the full expression for the intensity of the scattered signal

$$\begin{aligned}
I_{VV}^{\parallel\parallel} &\propto \int_0^{\frac{\pi}{2}}\int_0^{2\pi} I_{\mathrm{in}}|\boldsymbol{E}\cdot\boldsymbol{\mu}_{\shortparallel}|^2\, I_{\mathrm{sc}}|\boldsymbol{\mu}_{\shortparallel}\cdot\boldsymbol{E}|^2\rho(\varphi)d\gamma d\varphi \\
&\propto \int_0^{\frac{\pi}{2}}\int_0^{2\pi} (-\sin\theta\sin\varphi\cos\gamma + \cos\theta\cos\varphi)^4\rho(\varphi)d\gamma d\varphi \\
&\propto \int_0^{\frac{\pi}{2}}\int_0^{2\pi} \big(\sin^4\theta\sin^4\varphi\cos^4\gamma + \cos^4\theta\cos^4\varphi \\
&\quad + 6\sin^2\theta\cos^2\theta\sin^2\varphi\cos^2\varphi\cos^2\gamma - 4\sin\theta\cos^3\theta\sin\varphi\cos^3\varphi\cos\gamma \\
&\quad - 4\sin^3\theta\cos\theta\sin^3\varphi\cos\varphi\cos^3\gamma\big)\rho(\varphi)d\gamma d\varphi,
\end{aligned} \tag{4}$$

which simplifies to

$$I_{VV}^{\parallel\parallel} \propto 2\cos^4\theta\left\langle\cos^4\varphi\right\rangle + 6\cos^2\theta\sin^2\theta\left\langle\sin^2\varphi\cos^2\varphi\right\rangle + \tfrac{3}{4}\sin^4\theta\left\langle\sin^4\varphi\right\rangle. \tag{5}$$

Similarly, the $I_{VV}^{\perp\perp}$ case becomes

$$\begin{aligned} I_{VV}^{\perp\perp} &\propto \int_0^{\frac{\pi}{2}} \int_0^{2\pi} \int_0^{2\pi} I_{in} |\boldsymbol{E}\cdot\boldsymbol{\mu}_{\perp}|^2 \, I_{sc} |\boldsymbol{E}\cdot\boldsymbol{\mu}_{\perp}|^2 \rho(\varphi) \; d\zeta d\gamma d\varphi \\ &\propto (8 - 28\sin^2\theta + 23\sin^4\theta) \left\langle \sin^4\varphi \right\rangle \\ &\quad + (32\sin^2 - 40\sin^4\theta) \left\langle \sin^2\varphi \right\rangle + 8\sin^4\theta. \end{aligned} \tag{6}$$

We use a similar approach to obtain the polarization dependence for the two VH cases:

$$\begin{aligned} I_{VH}^{\shortparallel\shortparallel} &\propto \int_0^{\frac{\pi}{2}} \int_0^{2\pi} I_{in} |\boldsymbol{E}\cdot\boldsymbol{\mu}_{\shortparallel}|^2 \, I_{sc} |\boldsymbol{f}\cdot\boldsymbol{\mu}_{\shortparallel}|^2 \rho(\varphi) \; d\gamma d\varphi \\ &\propto \tfrac{3}{4}\sin^2\theta\cos^2\theta \left\langle \sin^4\varphi \right\rangle + 2\cos^2\theta\sin^2\theta \left\langle \cos^4\varphi \right\rangle \\ &\quad + (\sin^4\theta + \cos^4\theta - 4\sin^2\theta\cos^2\theta) \left\langle \sin^2\varphi\cos^2\varphi \right\rangle, \end{aligned} \tag{7}$$

where $\boldsymbol{f} = (-\cos\theta, 0, -\sin\theta)$ denotes the orientation of a polarizer for observing the scattered light, and is perpendicular to the incident light polarization.

$$\begin{aligned} I_{VH}^{\perp\perp} &\propto \int_0^{\frac{\pi}{2}} \int_0^{2\pi} \int_0^{2\pi} I_{in} |\boldsymbol{E}\cdot\boldsymbol{\mu}_{\perp}|^2 \, I_{sc} |\boldsymbol{f}\cdot\boldsymbol{\mu}_{\perp}|^2 \rho(\varphi) \; d\zeta d\gamma d\varphi \\ &\propto 4 - 6\sin^2\theta\cos^2\theta + 3(27\sin^2\theta\cos^2\theta - 4) \left\langle \cos^4\varphi \right\rangle \\ &\quad + 2(4 - 21\sin^2\theta\cos^2\theta) \left\langle \cos^2\varphi \right\rangle. \end{aligned} \tag{8}$$

As shown in Refs. [6] and [14], the anisotropy can be determined from optical obsorption for orthogonal polarizations. The absorption cross sections of SWNTs both parallel and perpendicular to the nanotube axis are noted as $\Lambda_{\shortparallel}$ and $\Lambda_{\perp}$. Experimentally, the absorption of incident light parallel ($I_{exp}(\theta = 0)$) and perpendicular ($I_{exp}(\theta = \frac{\pi}{2})$) to the alignment direction are measured to obtain the anisotropy using the following equation

$$\frac{I_{exp}(0) - I_{exp}(\frac{\pi}{2})}{I_{exp}(0) + 2_{exp}I(\frac{\pi}{2})} = \frac{\Lambda_{\shortparallel} - \Lambda_{\perp}}{\Lambda_{\shortparallel} + 2\Lambda_{\perp}} \left(\frac{3\left\langle \cos^2\varphi - 1 \right\rangle}{2} \right) = \frac{\Lambda_{\shortparallel} - \Lambda_{\perp}}{\Lambda_{\shortparallel} + 2\Lambda_{\perp}} S. \tag{9}$$

$S = \frac{1}{2}\left(3\left\langle \cos^2\varphi \right\rangle - 1\right)$ is the *nematic order parameter*, which indicates the degree of alignment of the sample. If the absorption cross sections $\Lambda_{\shortparallel}$ and $\Lambda_{\perp}$ are known, the order parameter S and distribution $\rho(\varphi)$ can be obtained and applied to our polarization-dependent Raman scattering studies.

B. RBM peak dependence of polarization angle

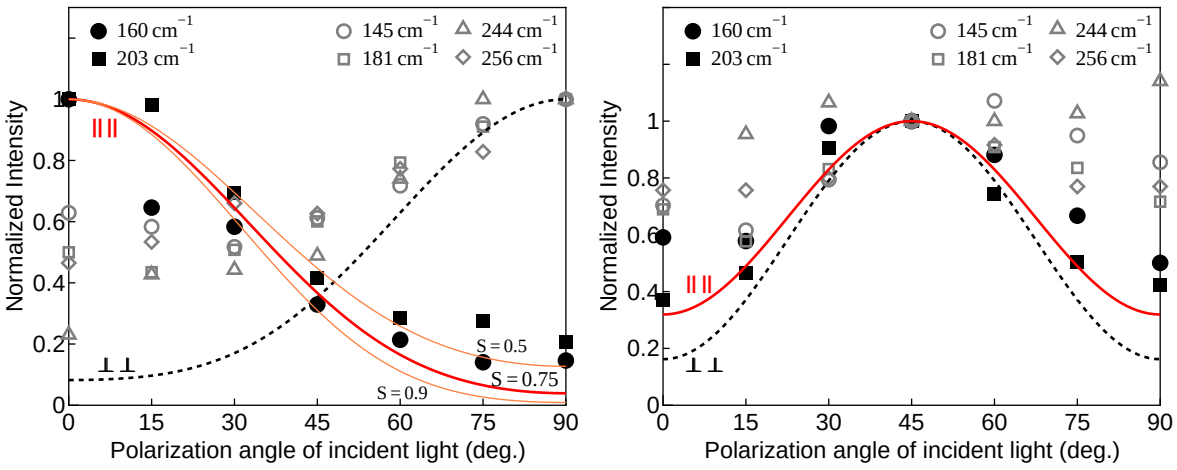

FIG. 8: (Color online) RBM peak intensities for incident light polarization angles from 0° to 90° with respect to the VA-SWNT alignment direction. Both VV (left) and VH (right) configurations are shown.

C. Polarized Raman spectra of stretch-aligned SWNTs in PVA

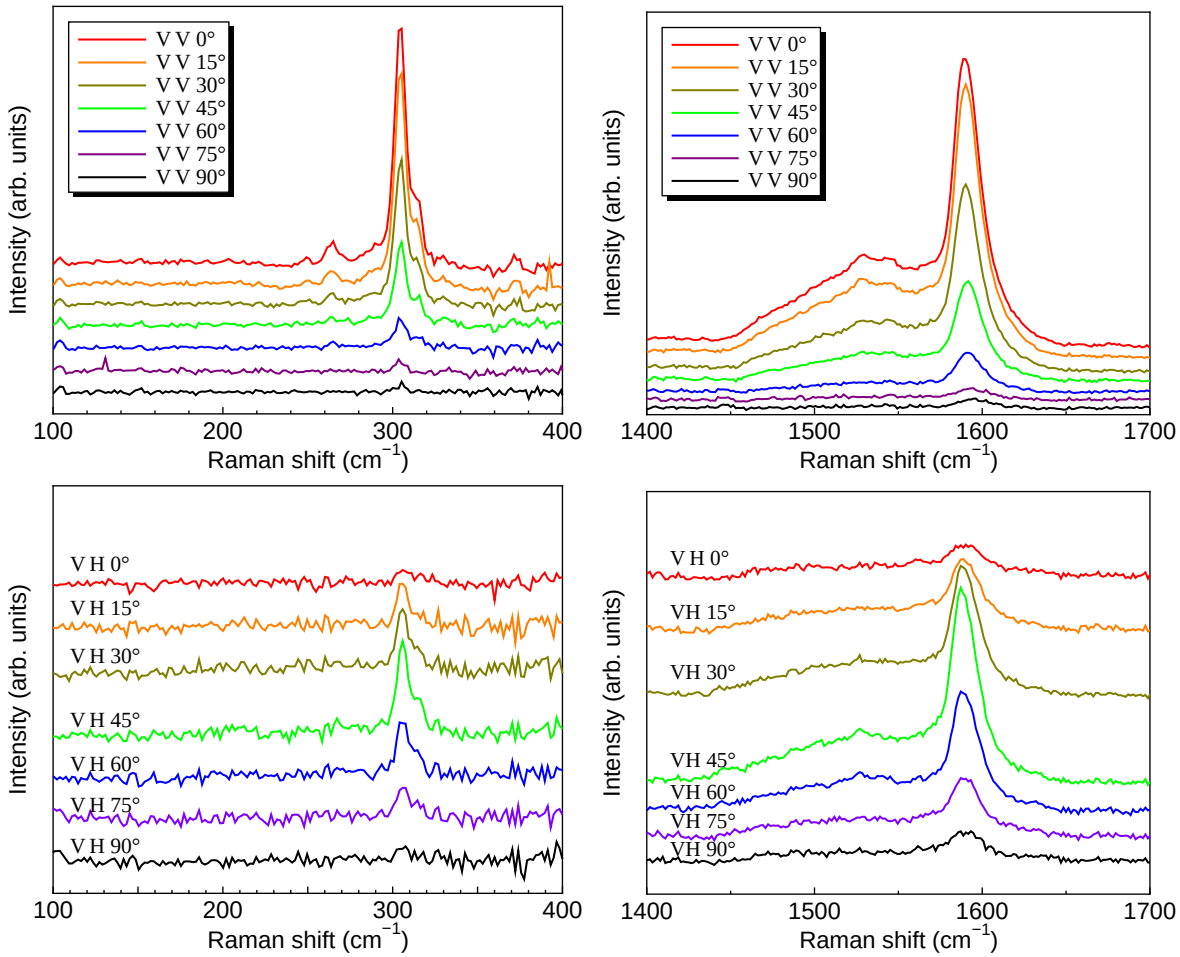

FIG. 9: (Color online) RBM (left) and G-band (right) Raman spectra of CoMoCat-PVA arrays with the incident polarization changing from 0° (along stretching direction) to 90° (perpendicular to the stretching direction). Spectra are shown for both VV (upper panels) and VH orientations (lower panels).

D. Laser heating effects

When measuring Raman spectra the SWNT sample can be heated considerably by the incident laser. It has been found that the anharmonic components of bonding become prominent at high temperature, which induce thermal expansion and thus decrease the Raman shift frequency.[16] All six components of the G-band behave in this way, decreasing

in frequency with increasing temperature. For SWNTs in general, the position of the G^+ peak is described by the function[16]

$$\omega(T) = \omega_0 - \frac{A}{\exp(B\hbar\omega_0/k_BT) - 1}, \tag{10}$$

where $\hbar$ is Planck's constant, k_B is Boltzmann's constant, T is the sample temperature, $\omega_0 = 1594$ cm^{-1}, $A = 38.4$ cm^{-1}, and $B = 0.438$. Therefore, the sample temperature can be inferred directly from the G^+ peak position. The temperature change also affects the peak intensity, which can be described by

$$I = I_0 \ \exp\left(-\frac{T}{B}\right). \tag{11}$$

Here, T is the sample temperature, I_0 denotes the Raman intensity at 0 K, and B is a fitting parameter (here, $B = 430$).

In the polarized measurements presented here, the G-band peaks were found to slightly increase in frequency when the incident polarization angle changed from 0° to 90°. This is because SWNTs more strongly absorb light that is polarized along the tube axis, which causes heating of the entire array. For the VV configuration, the G^+ peak changed from 1587.5 to 1591.5 cm^{-1}. Using Eq. (10), the sample temperature is found to be approximately 500 K at 0° and 360 K at 90°. For the VH configuration, the G^+ peak frequency shows a similar trend, shifting from 1587.5 to 1590 cm^{-1}. After correcting for this heating effect (not shown), the G^+ peak intensities are in better agreement with the intensity calculations for both VV and VH configurations.

To determine the effect of heating on RBM intensities, we measured Raman spectra with various laser powers and determined the temperature from the G^+ peak position. We then normalized the spectra after correcting for the temperature-induced decrease in G^+ intensity. Since increasing laser power not only increases the sample temperature but also increases the Raman intensity, it is necessary to remove the effect of laser power to obtain the real intensity dependence on temperature. Noting that G^+ and RBM peaks are similarly affected by laser power, this effect can be corrected for by normalizing with the temperature-corrected G^+ peak intensity.

The temperature dependence on peak intensity for the four main RBM peaks is shown in Fig. 10. The {181 cm^{-1}} group peaks decrease almost linearly by about 80% until 720 K, then become constant at higher temperatures. Chiashi *et al.*[16] similarly reported two different temperature-dependent intensity trends for HiPCO SWNTs, but in their case some

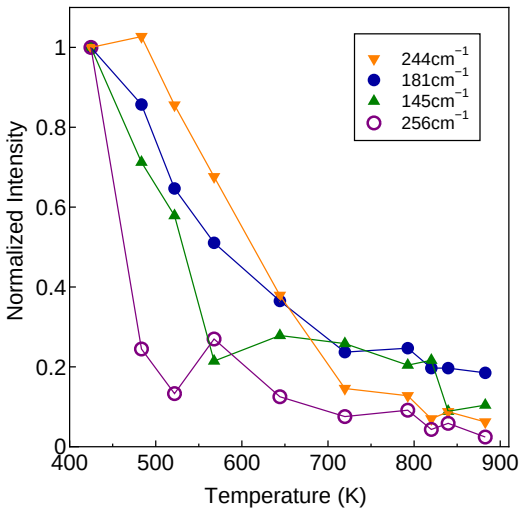

FIG. 10: (Color online) Temperature dependence of RBM peak intensities for VA-SWNTs.

peak intensities were also found to increase. Regardless of this difference, we can use the trends seen in Fig. 10 to obtain the correct polarization-dependent intensity relationship (the corrected form of Fig. 8). This is shown for the VV configuration used to obtain the data plotted in Fig. 4.

E. SEM image of SWNT array

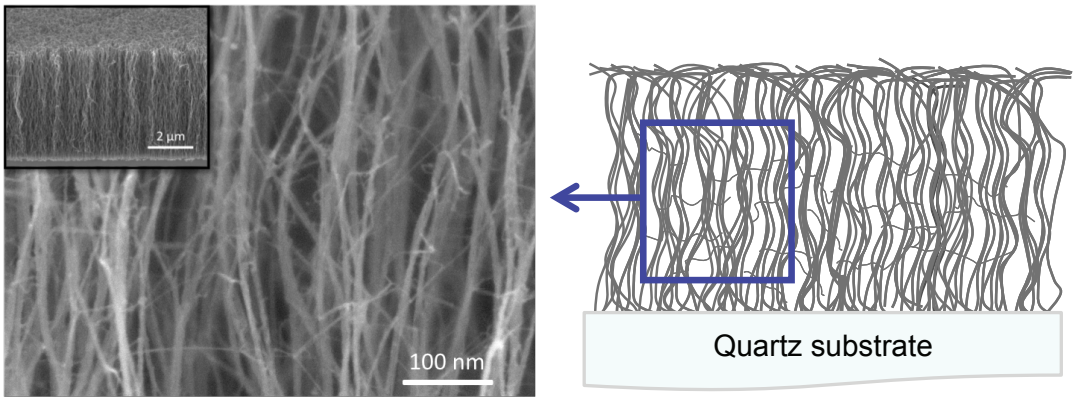

FIG. 11: (Color online) (Left) High-resolution SEM image of the middle part of a VA-SWNT array (inset: low magnification), and (Right) a scheme illustrating the morphology of the VA-SWNT array based on SEM observation

* Electronic address: maruyama@photon.t.u-tokyo.ac.jp

[1] R. Saito, G. Dresselhaus, and M.S. Dresselhaus, *Physical Properties of Carbon Nanotubes* (Imperial College Press, London, 1998).

[2] Y. Miyauchi, M. Oba, and S. Maruyama, Phys. Rev. B **74**, 205440 (2006).

[3] J. Lefebvre and P. Finnie, Phys. Rev. Lett. **98**, 167406 (2007).

[4] A. Grüneis, R. Saito, J. Jiang, Ge.G. Samsonidze, M.A. Pimenta, A. Jorio, A.G. Souza Filho, G. Dresselhaus, and M.S. Dresselhaus, Chem. Phys. Lett. **387**, 301 (2004).

[5] M.F. Islam, D.E. Milkie, C.L. Kane, A.G. Yodh, and J.M. Kikkawa, Phys. Rev. Lett. **93**, 037404 (2004).

[6] Y. Murakami, E. Einarsson, T. Edamura, and S. Maruyama, Phys. Rev. Lett. **94**, 087402 (2005).

[7] C. Kramberger, R. Hambach, C. Giorgetti, M.H. Rümmeli, M. Knupfer, J. Fink, B. Büchner, L. Reining, E. Einarsson, S. Maruyama, et al., Phys. Rev. Lett. **100**, 196803 (2008).

[8] Y. Murakami, S. Chiashi, E. Einarsson, and S. Maruyama, Phys. Rev. B **71**, 085403 (2005).

[9] S. Maruyama, R. Kojima, Y. Miyauchi, S. Chiashi, and M. Kohno, Chem. Phys. Lett. **360**, 229 (2002).

[10] F. Wang, G. Dukovic, L.E. Brus, and T.F. Heinz, Science **308**, 838 (2005).

[11] A. Jorio, M.S. Dresselhaus, and G. Dresselhaus, eds., *Carbon Nanotubes: Advanced Topics in the Synthesis, Structure, Properties and Applications* (Springer, 2008).

[12] Y. Murakami, S. Chiashi, Y. Miyauchi, M. Hu, M. Ogura, T. Okubo, and S. Maruyama, Chem. Phys. Lett. **385**, 298 (2004).

[13] S. Maruyama, E. Einarsson, Y. Murakami, and T. Edamura, Chem. Phys. Lett. **403**, 320 (2005).

[14] Y. Murakami, E. Einarsson, T. Edamura, and S. Maruyama, Carbon **43**, 2664 (2005).

[15] C. Kramberger, H. Shiozawa, H. Rauf, A. Grüneis, M.H. Rümmeli, T. Pichler, B. Büchner, D. Batchelor, E. Einarsson, and S. Maruyama, Phys. Stat. Sol. (b) **244-11**, 3978 (2007).

[16] S. Chiashi, Y. Murakami, Y. Miyauchi, and S. Maruyama, Jpn. J. Appl. Phys. **47**, 2010 (2008).

[17] P.T. Araujo, S.K. Doorn, S. Kilina, S. Tretiak, E. Einarsson, S. Maruyama, H. Chacham, M.A. Pimenta, and A. Jorio, Phys. Rev. Lett. **98**, 067401 (2007).

[18] C. Fantini, A. Jorio, M. Souza, M.S. Strano, M.S. Dresselhaus, and M.A. Pimenta, Phys. Rev. Lett. **93**, 147406 (2004).

[19] H. Kataura, T. Ueno, Y. Miyata, K. Yanagi, S. Okubo, S. Suzuki, and Y. Achiba, in *Proceedings of the 20th International Conference on Raman Spectroscopy* (2006).

[20] A. Jorio, G. Dresselhaus, M.S. Dresselhaus, M. Souza, M.S.S. Dantas, M.A. Pimenta, A.M. Rao, R. Saito, C. Liu, and H.M. Cheng, Phys. Rev. Lett. **85**, 2617 (2000).

[21] M.S. Dresselhaus, G. Dresselhaus, R. Saito, and A. Jorio, Phys. Rep. **409**, 47 (2005).